

On the birth of structural and crystallographic fabric signals in polar snow: A case study from the EastGRIP snowpack - APPENDIXES

Maurine Montagnat^{1,2*}, Henning Löwe³, Neige Calonne², Martin Schneebeli³, Margret Matzi³ and Matthias Jaggi³

¹ Univ. Grenoble Alpes, CNRS, IGE, F-38000 Grenoble, France

² Univ. Grenoble Alpes, Université de Toulouse, Météo-France, CNRS, CNRM, Centre d'Études de la Neige, F-38000 Grenoble, France

³ WSL Institute for Snow and Avalanche Research SLF, Davos Dorf, Switzerland

Correspondence*:

M. Montagnat

maurine.montagnat@univ-grenoble-alpes.fr

ABSTRACT

The role of near-surface snow processes for the formation of climate signals through densification into deep polar firn is still barely understood. To this end we have analyzed a shallow snow pit (0-3 meters) from EastGRIP (Greenland) and derived high-resolution profiles of different types of mechanically relevant fabric tensors. The structural fabric, which characterizes the anisotropic geometry of ice matrix and pore space, was obtained by X-ray tomography. The crystallographic fabric, which characterizes the anisotropic distribution of the **c**-axis (or optical axis) orientations of snow crystals, was obtained from automatic analysis of thin sections. The structural fabric profile unambiguously reveals the seasonal cycles at EastGRIP, as a consequence of temperature gradient metamorphism, and in contrast to featureless signals of parameters like density or specific surface area. The crystallographic fabric profile unambiguously reveals a signal of cluster-type texture already at shallow depth. We make use of order of magnitude estimates for the formation time of both fabric signals and discuss potential coupling effects in the context of snow and firn densification.

Keywords: Snow cover, Structural fabric, Crystallographic fabric, Seasonal signal, Metamorphism, Densification, Greenland

APPENDIX A: ORDER-OF-MAGNITUDE MODELLING OF THE EVOLUTION OF THE STRUCTURAL ANISOTROPY

For an order of magnitude estimate of the variations of the structural anisotropy, we consider the rate-equation model as proposed in (Leinss et al., 2020). In the absence of strain measurements, we solely focus here on the impact of temperature gradient metamorphism (TGM) and ignore contributions from settling by setting. In this case, the differential equation for the anisotropy A is given by

$$\frac{d}{dt}A(t) = \dot{A}_{\text{TGM}}(T(t), \nabla T(t)), \quad A(0) = A_0 \quad (1)$$

where A is related to the ratio of the correlation lengths via $\epsilon = (2 - A)/(2 + A)$. For the purpose below, we formalize the solution of the differential equation (1) in the form

$$A(t) = A(\{T(t'), \nabla T(t')\}_{t_0 < t' < t} | t_0, A_0). \quad (2)$$

as the anisotropy time series from t_0 to t for given temperature history $\{T(t'), \nabla T(t')\}_{t_0 < t' < t}$ and initial condition A_0 , that makes the dependence on involved quantities explicit.

As a first test, the anisotropy can be directly calculated from temperature and temperature gradient time series extracted from the measurements at different depths (Figure 1 (a)). Since the measurements include only one year, we simply apply a periodic continuation for all temperatures to another year. Then, the anisotropy time series per layer is computed via numerical integration of the equation (1) from $t_0 = 0$ to $t = 2$ years with initial condition $A_0 = 0$ and time step of 1 h. The results are shown in Figure 2 (a). They indicate that the typical increase of the temperatures and temperature gradients in the near-surface in summer are sufficient to explain seasonal jumps in ϵ of up to 0.3 solely as a consequence of near-surface metamorphism. Note that temperature data were taken *as is* on input for the numerical solution.

Indeed the simple argument above fully neglects the fact that material elements are buried in the course of time and thereby change their temperature and gradient history. A simple numerical experiment (using the measured temperatures) can be made by assuming that the z position of material elements are strictly advected into the sub-surface from their initial position at z_0 at time t_0 under a constant accumulation rate \dot{b} according to $z(t|z_0, t_0) = z_0 + \dot{b}(t - t_0)$. The age of a material element found at z at time t is then simply given by $a(z) = z/\dot{b}$. If the (spatio-temporal) temperature measurements are denoted by $T_m(z, t)$, then a structural anisotropy profile $A(z, t)$ at time t can be computed via

$$A(z, t) = A(\{T_m(z(t'|0, t' - a(z_0)), t'), \nabla T_m(z(t'|0, t' - a(z_0)), t')\}_{t - a(z) < t' < t} | t - a(z), 0) \quad (3)$$

In other words, the temperature and gradient history in equation (3) for calculating the anisotropy at depth z is obtained by following the space-time trajectory of a firn-parcel from the initial time $t - a(z)$ where the material element was at the surface with initial condition $A_0 = 0$. To calculate equation (3) by numerical integration, temperatures and gradients along the material trajectory were computed by 2D (spatio-temporal) interpolation of the measured data using the `scipy` function `RegularGridInterpolator`. The results are shown in Figure 2.

APPENDIX B: RE-ANALYSIS DATA OF MONTHLY AVERAGED PRECIPITATION AT EASTGRIP

Re-analyses have been performed over Greenland in the frame of an inter-comparison exercise (covered period 1979 - 2018), see (Fettweis et al., 2020). They are used here to extract the monthly averaged precipitation at EastGRIP. MAR (Modèle Atmosphérique Régional) is a limited area climate model which has been developed for the polar regions. It is based on the fully compressible equations of atmospheric dynamics with the hydrostatic assumption. It also contains detail descriptions of cloud microphysics and the snow pack. More details may be found in (Gallée et al., 2015) and references therein. Figure 3 provides the extracted data over the period of interest in this work, 2009 - 2017.

APPENDIX C: ORDER-OF-MAGNITUDE MODELLING OF THE EVOLUTION OF CRYSTALLOGRAPHIC ANISOTROPY

For sake of simplicity we suppose that individual snow grains deform plastically under a compression load applied from the above snowpack. The vertical component of the compression load can be estimated as:

$$\sigma_{zz} = \int_{z_0}^z \rho g dz \quad (4)$$

with ρ the snow density, and $g = 9.8 \text{ m s}^{-2}$. Here, we consider the viscoplastic deformation of snow grains, therefore, only the deviatoric part of σ , $S_{ij} = \sigma_{ij} - p\delta_{ij}$ is to be taken into account, with (i,j) as (x,y,z) and $p = \frac{\sigma_{zz}}{3}$ the isotropic pressure. At a depth $z = 2 \text{ m}$, with an average snow density of 350 kg m^{-3} , $S_{zz} = 4573 \text{ Pa}$.

Let's now consider an individual snow crystal with its **c**-axis oriented at an angle θ from the vertical direction (see scheme on Figure 4). Owing to the strong viscoplastic anisotropy of ice (Duval et al., 1983), we can assume that this crystal will deform only by dislocations gliding in the basal plane, the crystallographic plane perpendicular to the **c**-axis. From (Alley, 1988), during a strain increment $\Delta\varepsilon$ the crystal rotates of $\Delta\theta = \Delta\varepsilon \frac{\sin\theta}{\cos\theta}$. The Orowan equation further relates the strain rate to the dislocation activity (density of mobile dislocations d_m and velocity v_d), and Shearwood and Whitworth (1991) provide a relation between the mobile dislocation velocity and the resolved shear stress in the basal plane ($\tau = S_{zz} \cos\theta \sin\theta$), with a Arrhenius type of dependency on temperature. The rotation of an individual crystal follows equation 5, with parameters given in table 1.

$$\begin{aligned} d\varepsilon &= d_m b K(T) \tau dt \\ d\theta &= d_m b K(T) S_{zz} \sin^2(\theta) dt \end{aligned} \quad (5)$$

A simple test of this phenomenological model has been done by considering the assumption of a

Table 1. Parameters used for the grain rotation calculation. Only screw dislocations are considered and $K_{screw}(T)$ is taken from (Shearwood and Whitworth, 1991).

$d_m(\text{min})$ m^{-2}	$d_m(\text{max})$ m^{-2}	$K_{screw}(-20^\circ\text{C})$ $\mu\text{m s}^{-1}\text{MPa}^{-1}$	$K_{screw}(-40^\circ\text{C})$ $\mu\text{m s}^{-1}\text{MPa}^{-1}$	$S_{zz}(2\text{m})$ kPa	b m
10^6	10^8	1	0.01	4.57	4.5×10^{-10}

homogeneous stress (also called Sachs approximation (Sachs, 1928)) applied to all the grains in a 1 m^3 volume located below the 2 m depth EastGRIP snow pack. This approximation, that does not guaranty the strain compatibility between grains, appears as a reasonable first approximation in the frame of a low density snow pack but should, of course, be reconsidered when dealing with increasing density.

To estimate the evolution of texture of the snow grains, an initial population of 1000 randomly oriented grains was considered. The texture evolution with time was followed by using the $a_1^{(2)}$ eigenvalue of the second order orientation tensor $\mathbf{a}^{(2)}$.

We considered an initial mobile dislocation density randomly varying between $d_m = 10^6$ and $d_m = 10^8 \text{ m}^{-2}$ (Higashi, 1988), and an enhancement factor E for local stress concentration varying randomly between 1 and 10 (Hagenmuller et al., 2014). Several trials were done to obtain a range of evolution. Figure 5 (a), that represents the evolution of $a_1^{(2)}$ as a function of time for a temperature relevant to EastGRIP (-20°C) and a temperature relevant to Point Barnola (-40°C), illustrates the fact that temperature has a strong impact

on dislocation mobility, and therefore on the c-axis rotation with strain. In particular, it is shown that the crystallographic fabric of the snow grain population considered can reach anisotropy of the order of magnitude of the one measured in the third meter of the EastGRIP snow pack after about 8 to 11 years, in the temperature conditions relevant to EastGRIP. On the contrary, too low temperatures reduce the dislocation mobility to the point that individual grain rotation is inhibited at the time scale considered. The choice of the initial mobile dislocation density range has a strong impact on the anisotropy evolution but can not be constrained more than based on values obtained on ice single crystals.

REFERENCES

- Leinss S, Löwe H, Proksch M, Kontu A. Modeling the evolution of the structural anisotropy of snow. *The Cryosphere* **14** (2020) 51–75. doi:10.5194/tc-14-51-2020.
- Fettweis X, Hofer S, Krebs-Kanzow U, Amory C, Aoki T, Berends CJ, et al. GrSMBMIP: Intercomparison of the modelled 1980-2012 surface mass balance over the greenland ice sheet. *The Cryosphere Discuss.* **2020** (2020) 1–35. doi:10.5194/tc-2019-321.
- Gallée H, Preunkert S, Argentini S, Frey MM, Genthon C, Jourdain B, et al. Characterization of the boundary layer at dome c (east antarctica) during the opale summer campaign. *Atmos. Chem. Phys.* **15** (2015) 6225–6236. doi:10.5194/acp-15-6225-2015.
- Duval P, Ashby M, Anderman I. Rate controlling processes in the creep of polycrystalline ice. *J. Phys. Chem.* **87** (1983) 4066–4074.
- Alley RB. Fabrics in polar ice sheets - Development and prediction. *Science* **240** (1988) 493–495.
- Shearwood C, Whitworth RW. The velocity of dislocations in ice. *Phil. Mag.* **A64** (1991) 289–302.
- Sachs G. Zur Ableitung einer Fliessbedingung. *Z. Verein Deutscher Ing.* **72** (1928) 734–736.
- Higashi A. *Lattice defects in ice crystals* (Hokkaido University Press, Sapporo Japan) (1988).
- Hagenmuller P, Theile TC, Schneebeli M. Numerical simulation of microstructural damage and tensile strength of snow. *Geophysical Research Letters* **41** (2014) 86–89. doi:10.1002/2013GL058078.

FIGURES

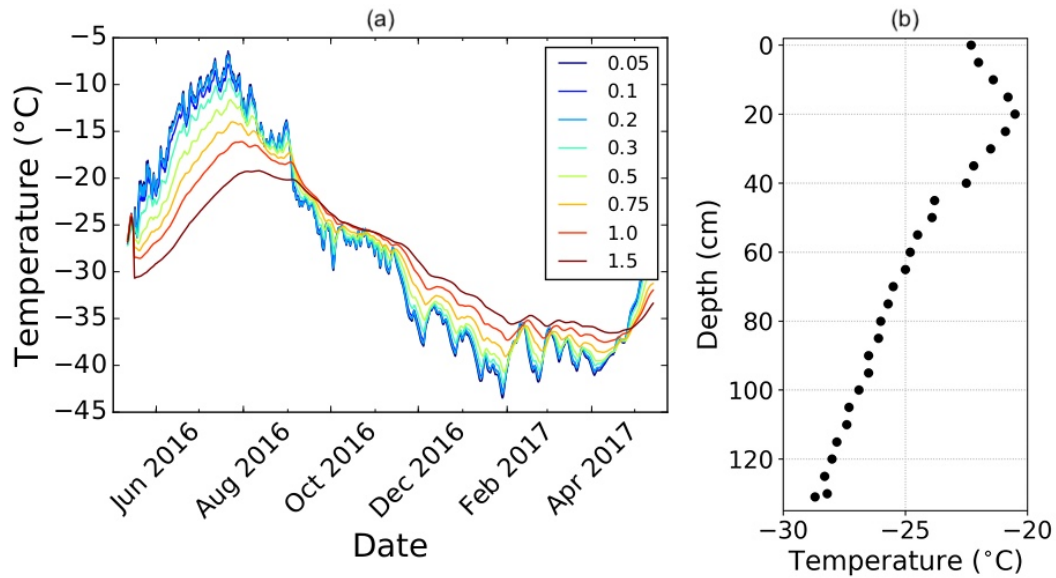


Figure 1. [Figure 2 in main text] (a) Temperature data (Courtesy of H-C. Steen-Larsen) measured from April 2016 to March 2017 at different depths in m (legend). (b) Temperature profile of the first 1.3 m depth of the snowpack measured at EastGRIP on May 24th, 2016.

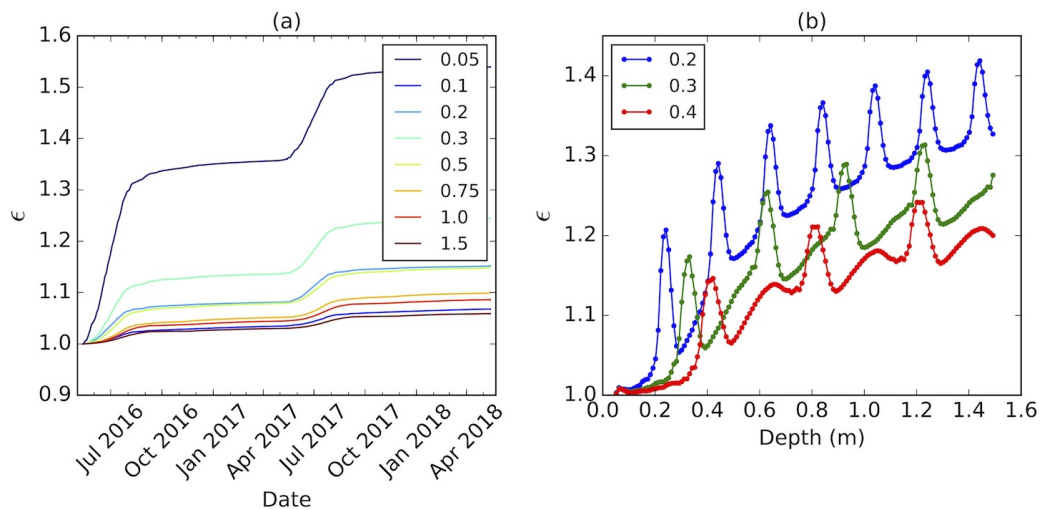


Figure 2. [Figure 8 in main text] (a): Modeled evolution of the structural anisotropy ϵ over two years with temperature and temperature gradient time series taken from the EastGRIP field measurements at fixed depth in m (legend). (b): Modeled anisotropy profile using spatio-temporal interpolation of the measured temperatures and gradients for different (constant) accumulation rates in m/year (legend). The start of the time series in (a) and the surface (b) corresponds to May 12. For details see text.

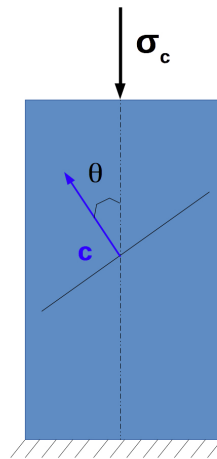


Figure 4. [Figure 10 in main text] Schematic view of the loading state of the single crystal. c is the c -axis orientation.

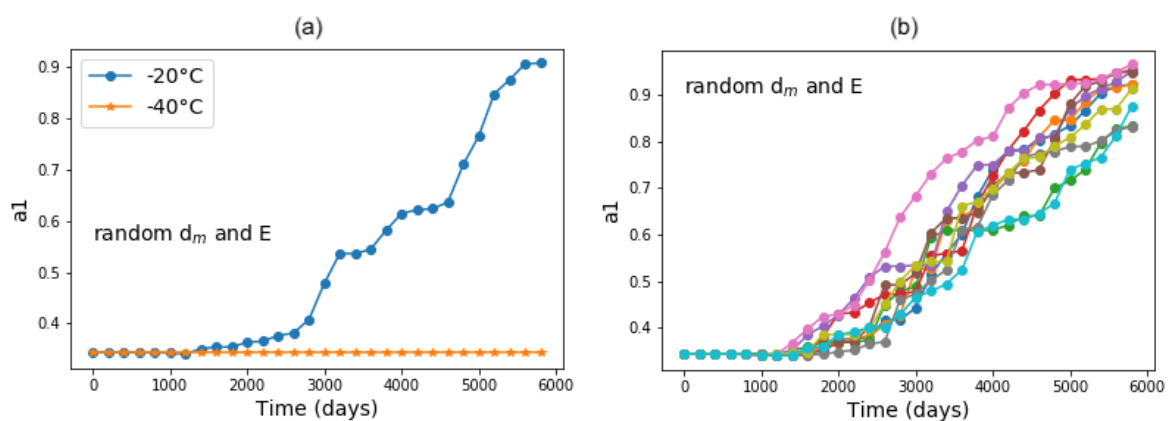


Figure 5. [Figure 11 in main text] Modeled evolution of $a_1^{(2)}$ as a function of time, based on 1000 random initial orientations, following the homogeneous stress hypothesis (Sachs), with initial density varying randomly between $d_m(\min)$ and $d_m(\max)$ (table 1) and stress concentration E varying randomly between 1 and 10. (a) Comparison between the two temperature conditions of Point Barnola (-40°C) and EastGRIP (-20°C) for on single run. (b) 10 runs performed for EastGRIP conditions (-20°C). No variation between the runs is observed for Point Barnola conditions.